Computer-Assisted Registration, Segmentation, and 3D Reconstruction from Images of Neuronal Tissue Sections

Ingrid Carlbom, *Member, IEEE,* Demetri Terzopoulos, *Member, IEEE,* and Kristen M. Harris

Abstract— **Neuroscientists have studied the relationship between nerve cell morphology and function for over a century. To pursue these studies, they need accurate three-dimensional models of nerve cells that facilitate detailed anatomical measurement and the identification of internal structures. Although serial transmission electron microscopy has been a source of such models since the mid 1960s, model reconstruction and analysis remain very time consuming. We have developed a new approach to reconstructing and visualizing 3D nerve cell models from serial microscopy. An interactive system exploits recent computer graphics and computer vision techniques to significantly reduce the time required to build such models. The key ingredients of the system are a digital "blink comparator" for section registration, "snakes," or active deformable contours, for semiautomated cell segmentation, and voxel-based techniques for 3D reconstruction and visualization of complex cell volumes with internal structures.**

I. Introduction

NEUROSCIENTISTS study the relationship between neuronal dendritic morphology and function by searching for links between morphology and behavior and between morphology and disease. Detailed morphological studies require accurate three-dimensional models of nerve cells that facilitate anatomical measurement and identification of internal structures. Neuronal dendrites and their protruding dendritic spines can be seen with a light microscope (Fig. 1), but the resolution is insufficient for detailed anatomical measurement and the internal structures are not visible. The preferred method for detailed measurement and study of internal cell structure is 3D reconstructions from serial electron microscopy, or serial EM (Fig. 2) [25], [24], [60], [70].

Reconstructions from serial EM have been produced almost since the invention of the electron microscope. Initially, the reconstructions were purely manual, but over the years they have relied increasingly on computers. Even with current computer-assisted techniques, the reconstruction of a 5 μm dendritic segment with all of its spines and synapses, along with the editing and quantitative analysis of the reconstructed model, can take months of work. By contrast, the tissue preparation and EM photography take only a few days! It is remarkable that so many neuronal reconstructions have been made because "... the incredible investment in time and energy necessary to reconstruct cells is nothing short of heroic" [60].

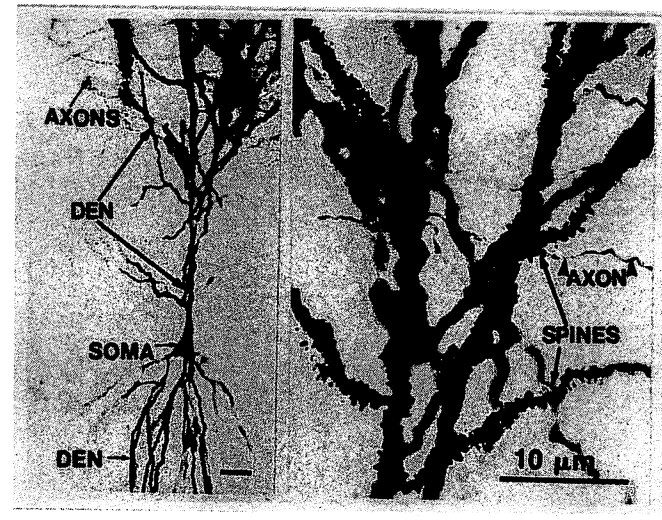

Fig. 1. A hippocampal pyramidal cell with the soma and the dendrites (den) visible. The axons are from other hippocampal cells that form synapses with these dendrites. At higher magnification the dendritic spines are seen protruding from the dendrite. Bars = 10 μm. (Reproduced from [23] with permission from the publisher.)

We are working towards a system that makes serial reconstruction a less time consuming process. A complete system would include the following five components: (1) rapid image entry; (2) image registration; (3) image segmentation; (4) 3D reconstruction and visualization; and (5) quantification. Our work has not yet addressed rapid image entry or quantification issues. Recent work indicates the possibility of rapid, high quality image acquisition by equipping electron microscopes with CCD imaging devices [1]. In the next section, we review the relevant neurophysiological motivation of our work, including possible quantification goals.

The present paper addresses components (2), (3), and (4). Specifically, we propose a new interactive approach to reconstructing and visualizing 3D nerve cell models from serial microscopy. Our prototype system exploits recent computer graphics and computer vision techniques to reduce significantly the time required to build the models. It features a digital "blink comparator" for section registration, "snakes," or active deformable contours, for semi-automated cell seg-

Manuscript received December 4, 1992. The associate editor responsible for coordinating the review of this paper and recommending its publication was S. M. Pizer.

I. Carlbom is with Digital Equipment Corporation, Cambridge Research Lab, Cambridge, MA 02139 USA.

D. Terzopoulos is with the Department of Computer Science, University of Toronto, Toronto, ON M5S 1A4 Canada.

K. M. Harris is with the Department of Neurology, Children's Hospital, Enders 260, Boston, MA 02115 USA.

IEEE Log Number 9401073.

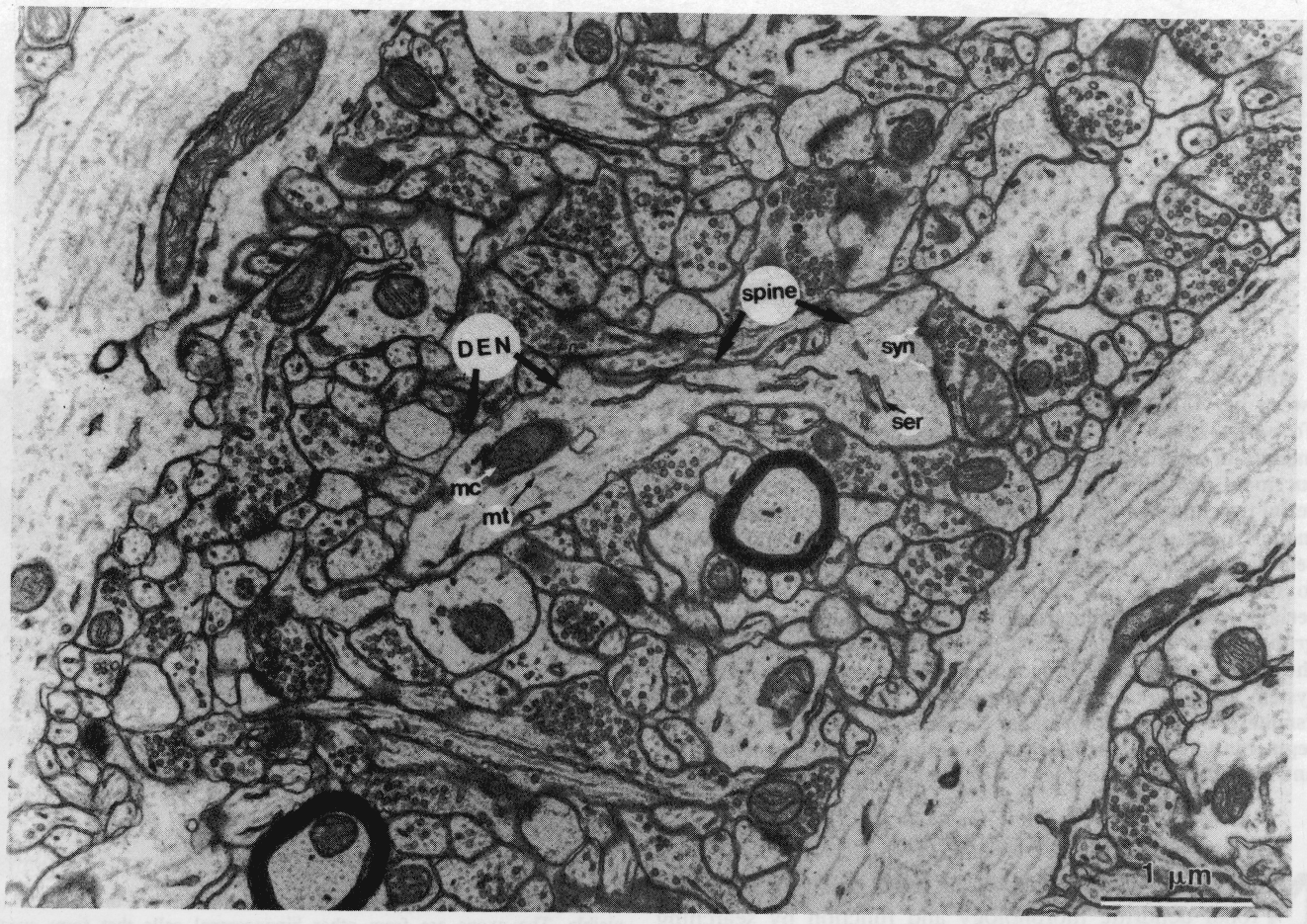

Fig. 2. An EM photomicrograph from a section of a rat hippocampus. The dendrite (den) is located in the center, and a large spine is protruding from its right side. The mitochondrion (mc), microtubules (mt), some smooth endoplasmic reticulum (ser), and the synapse (syn) are indicated. Bar = 1 μm.

mentation, and voxel-based techniques for 3D reconstruction and visualization of the 3D morphology of dendrites along with their internal structures.

A. Neurophysiological Motivation

A nerve cell, or neuron, has four constituent parts: the cell body (soma), the dendrites, the axon, and the presynaptic terminal of the axon [31]. The soma is the metabolic center of the cell, the dendrites are the receiving units, the axon is the conducting unit, and the presynaptic terminals are the transmitting units. The areas of contact between the presynaptic axonal terminals of one cell and the dendrites of another cell are called the synapses. Most excitatory synapses are located at the end of protrusions on the dendrites, called the dendritic spines (see Fig. 1).

In humans, the dendritic spines are lost or change shape both with aging [15] and with diseases that affect the nervous system, such as dementia [9], brain tumors [58], Down's syndrome [45], epilepsy [54], Huntington's disease [22], and alcoholism [16]. Detailed anatomical descriptions of the synapses and dendritic spines will provide new understanding about their function, thus improving opportunities for understanding the underlying causes and effects of these diseases.

The dendritic spine is positioned so that changes in its morphology could modulate the transfer of information from the synapse to the dendrite [5], [69]. Direct physiological study of the relationship between dendritic spine morphology and function has been impossible because of their small size. Several simulations with theoretical models have shown, however, that small changes in morphology could change the biophysical and biochemical properties of the spines [51], [35]. Several laboratory studies have shown that dendritic spines change shape during maturation, following experience, and in response to direct physiological stimulation of the presynaptic axon. Repeated, or "tetanic," stimulation causes an enhanced synaptic efficacy, which is referred to as long-term potentiation (LTP), a leading candidate for a synaptic explanation of behavioral learning [6]. Anatomical analyses of stimulated dendrites have revealed swollen spines and changes in the size of synapses (for a review see [24]). Thus, a change in morphology might contribute to, or represent, the increase in synaptic efficacy which is observed after stimulation.

Research has also shown that the cytoskeleton and the organelles internal to the neuron, such as neurofilaments, microtubules, mitochondria, and smooth endoplasmic reticulum (see Fig. 2) may control the shape of the nerve cell [36]. The challenge is to find links between neuronal morphology and physiological function in the normal and diseased brain [5].

B. Previous Work

This section reviews prior work on registration, reconstruction, segmentation, and visualization that is relevant to our research.

Registration and Reconstruction: Early EM reconstruction techniques were entirely manual [59]. A photograph from an electron microscope was illuminated and the outline of the structures of interest were traced on a sheet of acetate positioned on top of the print. Next a photograph of an adjoining section was illuminated and aligned with the trace from the previous section, and its structures were then traced on a new sheet of acetate. This process was repeated for all sections. The thickness of the acetate and the magnification were chosen so that a fairly accurate model would result by inserting a number of blank sheets of acetate between each trace. Finally, an artist would produce a 2D illustration of the 3D model.

Over the years, reconstruction from serial EM has become increasingly computer assisted. In a system developed by Stevens *et al.* [59], [60], the EM negatives are first rephotographed onto a 35 mm filmstrip. Next, the filmstrip is mounted on a film transport, which in turn is mounted on a stage driven by two computer-controlled stepping motors. The first image is digitized and stored in image memory. The second image is continually digitized while the user moves the film transport, and a video switcher alternately displays the stored and "live" images on a graphics screen at a frequency of about 4 Hz. There is an illusion of movement when the images are misaligned, and the movement is reduced as they are brought into alignment. When the motion is minimized between the two images or features of interest, the second image is stored. Next, serial sections two and three are aligned, followed by pairwise alignment of the remaining sections. Once all the images are aligned, the features or boundaries of interest are traced manually using a bitpad. The traces can be displayed as a set of contours, as contours with the hidden lines removed, or tessellated to form a surface which can be displayed as a solid object [26].

Using motion to compare photographs of the same or similar objects is not a new idea. Astronomers have used *blink comparators* since early this century to study astronomical plates [12]. A blink comparator holds two plates of the same part of the sky, and alternately displays them to the user. Stationary objects such as stars remain fixed, but objects such as comets or planets appear to move.

The problem of image alignment appears in many disciplines. Cartographers need to align aerial photographs, and in robot vision much effort is devoted to registration of stereo pairs and temporal image sequences [28]. In both these disciplines, the images are different views of the *same* object, and in robot vision one can often assume that, at least locally, images are only misaligned translationally. The alignment of neural sections, however, is a considerably more difficult problem because the EM images are misaligned both translationally and rotationally and there is generally a large discrepancy between consecutive images. The latter is due both to the integration over the thickness of the section in the EM photographic process and to distortions of the tissue by its preparation and by the EM process.

In addition to manual alignment techniques, such as the one described above for aligning neural slices, automatic registration methods based on cross correlation, control points (or landmarks), and moments are commonly applied to biomedical image registration [7]. Cross correlation and moment based techniques often require feature extraction through manual or automatic means, and control point based techniques often require manual identification of the control points. Cross correlation has been used to register retinal images [7] where edges of common features in adjoining images are employed in the correlation process. Giertsen *et al.* [21] proposed a method to align electron micrographs which uses both control points and moments. They manually trace the membrane and internal substructures of a pancreatic cell in serial sections and specify connectivity relations among successive contours. Using contour shape features (centroids and mean radii), they determine linear transformations between successive contours and refine the alignment using residuals between the original and smoothed data.

The registration of neural micrographs does not lend itself well to cross correlation or moment based techniques. One must use the entire section for registration in order to avoid overcompensating for structural changes in the dendrite between sections and for distortions introduced by the tissue preparation process. However, the dendrite, the object of interest, covers only a small area near the center of the neural section. Consequently, features required for correlation which may not be of interest during reconstruction would need to be extracted prior to registration. Unfortunately, existing automatic segmentation techniques experience difficulty in reliably extracting useful features from neural micrographs. Furthermore, there are no suitable landmarks in adjoining sections to provide exact correspondence. The semiautomatic method described by Giertsen *et al.* [21] would appear to require more effort than our manual approach to alignment, since we can limit segmentation to the object of interest and we can take advantage of the frame-to-frame coherence in the registered images during segmentation.

Segmentation: Many techniques have been developed for 2D and 3D biomedical image segmentation, and they may be categorized into statistical classification methods, region growing methods, and boundary methods. The simplest classification method, intensity thresholding, was employed in [29], while more sophisticated Bayesian estimation was applied in [13]. These techniques work relatively well for separating soft and hard tissue in CT scans. Region-based segmentation methods include multiresolution techniques such as those developed in [40], [18], [67]. A simple boundary-based method is iso-surface approximation. An example is the *marching cubes* technique [44], which constructs 3D polygonal representations of constant density surfaces from volumetric data by generating polygonal patches in a 3D grid using a table that classifies the 14 types of intersections that can occur between the iso-surface and cubes in the grid. Other boundary segmentation

techniques perform edge detection using various 3D edge detectors (e.g., [43], [48], [73], [30], [29]). A more sophisticated approach to segmenting MR scans proposed by Sander and Zucker [53] fits local quadric patches to Zucker-Hummel 3D operator responses using iterative optimization.

Unfortunately, because of the complexity of EM images of neuronal tissue (see Fig. 2), straightforward segmentation using any of the aforementioned techniques does not appear promising for 3D reconstruction of dendritic models. Therefore, we aim at introducing a higher level of automation into the section-by-section manual tracing methodology currently practiced by neuroscientists. A model-based image feature localization and tracking technique known as *snakes* [32] is well suited to this goal. Snakes are dynamic models that differ substantially from more mundane contouring approaches. Snakes are attracted to image boundaries through forces, which not only reduces the contouring time, but also increases the accuracy of the tracing.

The ability of snakes to conform to complex biological shapes such as cells and to track their nonrigid deformations across image sequences makes them attractive tools for biomedical image analysis. In [39], snakes are used to track living cells moving on a planar surface. Assuming modest interframe motion, snakes can exploit frame-to-frame coherence to track the moving cell and also follow the deformations which occur as the cell moves. Ayache *et al.* [2] use snakes to find edges in cross sections of MR data. The user draws an approximate contour around the region of interest and the snake deforms to fit the regions more accurately. Once the snake has reached an equilibrium, it is used as a starting point for the next cross section. A 3D model is built from the resulting set of contours using Delauney triangulation [3]. Variations on snakes based on B-splines have been applied to the segmentation of 3D CT and MR data [37]. Other model-based CT and MR data segmentation methods closely related to snakes include the Fourier curve models proposed by Duncan *et al.* [14] and the deformable templates of Lipson, Yuille, *et al.* [42].

Visualization: Volume visualization is used in applications in various disciplines, such as medicine, geophysics, molecular biology, atmospheric research, and industrial inspection [65]. Much work has been devoted to high-quality rendering of CT, PET and MR data [13], [38], seismic data [52], [72], and cellular microscopy data ([56], [33], [4]. Specialized software and hardware has been developed to facilitate real-time manipulation of both medical data [46], [47] and seismic data [10]. More recently, general-purpose software for volume rendering has become available. Examples are ISG Technologies' ICAR^{TM} System [61], the SYNU system from San Diego Microscopy and Imaging Resource [27], Advanced Visual Systems' AVS^{TM} system [66] and VitalImages' VoxelView^{TM} system [68]. Here, we used the VoxelView^{TM} system on a Silicon Graphics 4D/210GTX workstation to visualize the 3D reconstructed dendrites. We are also using an experimental ray-tracer implemented on a Digital Equipment Corporation DECmpp^{TM} 12000/Sx massively parallel computer.

II. Reconstruction of Neuronal Dendrites

A. Data Acquisition

Using routine tissue processing, a slice (400 μm thick) of well-preserved hippocampus was obtained from the brain of a male rat, and the slice was embedded in epoxy resin. The slice was further sectioned with an ultramicrotome, at an average section thickness of about 0.06 μm. (The dendritic segment used in this paper is dendrite number 24 of reference [26]). Each section was photographed at 10,000 times magnification in a JEOL 100B transmission electron microscope and printed on 8 × 10 inch photographic paper (see Fig. 2).

The EM photomicrographs were digitized on an ECRM Autokon flat-bed laser scanner capable of digitizing reflection copy images at a wide range of resolutions [64]. The scanner has a fixed spot size and the intensity can be quantized at one or eight bits/pixel. We digitized the images at a resolution of $2,560 \times 1,983$ pixels, approximately twice the sampling rate of the smallest features of interest, and with eight bits of intensity per pixel. The images were low-pass filtered and subsampled to a size of 640×496 pixels.

B. Image Registration

We chose a manual approach to image registration for two reasons. First, the automatic alignment of successive EM images is a very difficult problem, because the images are displaced both translationally and rotationally and usually there is a large disparity between consecutive images. Second, even if an automated solution can be found, user intervention will be necessary when the tissue has been distorted during preparation; for example, when a section has a fold.

We have implemented an interactive digital blink comparator. One image is held stationary and the user translates and rotates the other image while the stationary and moving images are alternately shown on a graphics screen. The user can translate the image in the x- and y-directions and can rotate the image about its center by using a three-button mouse, each button controlling one type of motion. The user moves the image until the motion between the two images is minimized and the images are aligned. By precomputing x- and y-components of the composite transformation, we obtain comparisons at a frequency of about 2.5 Hz for a 640 × 496 pixel image on a DECstation^{TM} 5000/240HX. We found this frequency adequate to obtain good alignment.

When all images are aligned by pairs, we find the composite rotation and translation transformation for each image relative to the first image in the EM series and resample the images using a spatially varying digital shift filter.

From sampling theory we know that in one dimension the impulse response of the ideal shift, or interpolation, filter is $\sin(\pi(m-T))/\pi(m-T)$, where m ranges over the sampling points, and T is the delay or, in our case, the fraction of a pixel [71]. Since this filter is of infinite duration, we window the *sinc* function with a raised cosine: $0.5 + 0.5 * \cos(2\,\pi m)/(L+1)$, where $|m| \leq (L-1)/2$, and L is the width of the window. (The raised cosine is sometimes referred to as a *Hanning* window [49] or a *Hann* window [71].) In order to select

a suitable L, we plot for several values of L the frequency response magnitude and phase for both the ideal shift filter and the finite duration impulse response (FIR) filter. We choose a value for L which gives good agreement between the desired frequency response and the actual frequency response in both magnitude and phase.

The two-dimensional filter used for resampling is the cascade of two one-dimensional FIR filters, with the horizontal filter interpolating in the x-direction and the vertical filter interpolating in the y-direction. Since this filter can give values that are outside the range of the input data, including negative values, we rescale the resampled image to the range [0, 255]. The resulting registered, resampled, and rescaled images are input to the segmentation process described in the next section.

C. Extracting Models from Electron Micrographs

The extraction of neuronal dendrites from a set of aligned EM images reduces to three subproblems: (1) the localization of dendritic profiles in digital micrographs; (2) the segmentation of the interiors of dendrites bounded by profiles; and (3) the identification of profiles of the same dendrite across serial micrographs. The density and geometric complexity of neuronal features in micrographs make the first and third subproblems especially difficult to automate fully.

We take a semiautomatic approach which exploits physically based vision techniques for interactively localizing and tracking extended features in images. We employ a variant of snakes, the interactive deformable contour models introduced in [32]. Snakes provide significant assistance to the user in accurately locating the membranes that bound the dendrites in EM images. Using a mouse, the user quickly traces a contour which approximates the dendrite boundary, then starts a dynamic simulation that enables the contour to locate and conform to the true membrane boundary under the influence of an image force field. Where necessary, the user may guide the contour by applying simulated forces using the mouse. Through minimal user intervention, snakes quickly produce accurate dendritic profiles in the form of complete, closed contours that facilitate the segmentation of dendritic interiors. Finally, with some guidance, snakes are able to exploit the coherence between serial micrographs to quickly extract a sequence of profiles of the same dendrite.

Deformable Contour Models: A snake can be thought of as a dynamic deformable contour in the x-y image plane. We define a discrete deformable contour as a set of n nodes indexed by $i = 1, \ldots, n$, with time varying positions $\mathbf{x}_i(t) = [x_i(t), y_i(t)]'$. The behavior of an interactive deformable contour is governed by the first-order dynamic system of equations

$$\gamma \frac{d\mathbf{x}_i}{dt} + \alpha_i + \beta_i = \mathbf{f}_i; \qquad i = 1, \ldots, n \tag{1}$$

where γ is a velocity-dependent damping constant, $\alpha_i(t)$ are "tension" forces which make the snake act like a series of springs that resist deformation, $\beta_i(t)$ are "rigidity" forces which make the snake act like a thin wire that resists bending, and $\mathbf{f}_i(t)$ are forces in the image plane applied to the contour.

Let l_i be the given reference length of the spring connecting node i to node $i+1$ and let $\mathbf{r}_i(t) = \mathbf{x}_{i+1} - \mathbf{x}_i$ be the separation of the nodes. Given the deformation $e_i(t) = \|\mathbf{r}_i\| - l_i$, we define

$$\alpha_i = \frac{a_i e_i}{\|r_i\|}\mathbf{r}_i - \frac{a_{i-1} e_{i-1}}{\|\mathbf{r}_{i-1}\|}\mathbf{r}_{i-1}. \tag{2}$$

It is convenient to create contours that can gradually stretch or shrink in a viscoelastic manner under a sustained applied force. A viscoelastic contour results from setting

$$\frac{dl_i}{dt} = \nu_i e_i \tag{3}$$

where ν_i is a coefficient of viscoelasticity.[1] To give the contours some rigidity, we introduce the variables b_i and define rigidity forces

$$\begin{aligned}\beta_i = {} & b_{i+1}(\mathbf{x}_{i+2} - 2\mathbf{x}_{i+1} + \mathbf{x}_i) - 2b_i(\mathbf{x}_{i+1} - 2\mathbf{x}_i + \mathbf{x}_{i-1}) \\ & + b_{i-1}(\mathbf{x}_i - 2\mathbf{x}_{i-1} + \mathbf{x}_{i-2}).\end{aligned} \tag{4}$$

Note that in the absence of external forces, if the nodes are separated more than l_i, are equally spaced, and lie on a straight line, α_i and β_i vanish and the contour will be at equilibrium. Tension and rigidity are locally adjustable through the a_i and b_i variables. In particular, by setting $a_i = b_i = 0$, we are able to break a long deformable contour into several shorter contours on an image.

To simulate the deformable contour we integrate the system of ordinary differential equations (1) forward through time using a semi-implicit Euler procedure [50]. Applying the forward finite difference approximation $d\mathbf{x}_i/dt \approx (\mathbf{x}_i^{t+\Delta t} - \mathbf{x}_i^t)/\Delta t$ to (1) and collecting linear terms in the $\mathbf{x}_i$ on the left yields the pentadiagonal system of algebraic equations

$$\frac{\gamma}{\Delta t}\mathbf{x}_i^{t+\Delta t} + \beta_i^{t+\Delta t} = \frac{\gamma}{\Delta t}\mathbf{x}_i^t - \alpha_i^t + \mathbf{f}_i^t \tag{5}$$

for the subsequent node positions $\mathbf{x}_i^{t+\Delta t}$ in terms of the current positions $\mathbf{x}_i^t$. Since the system has a constant coefficient matrix, we factorize it only once at the beginning of the deformable contour simulation using a direct LDU factorization method and then efficiently resolve with different right-hand sides at each time step (see [62] for details).

According to (3) we apply the viscoelastic update

$$l_i^{t+\Delta t} = l_i^t + \Delta t \nu_i e_i^t. \tag{6}$$

To speed up the simulation, it suffices to increase ν_i and perform the update only once every few time steps. Though experimentation, we have found that the parameter values $a_i = 1.0$, $b_i = 0.5$, $\gamma = 0.5$, $\nu_i = 1.0$, and viscoelastic updates once every 5 time steps ($\Delta t = 1$ is assumed) yields a rapid, stable simulation of deformable contours with appropriate physical behavior for our application. After each simulation time step we draw lines between the new node positions $\mathbf{x}_i^{t+\Delta t}$ to display the deformable contour as a dynamic curve in the image plane.

[1] Note that in [8] we employed deformable contours that stretch arbitrarily but resist compression past their initial lengths. After much experimentation in our application, we feel that viscoelastic contours perform better in our application.

Image Segmentation Using Deformable Contours: The deformable contour is responsive to an image force field which influences the contour's shape and motion. It is convenient to express the force field as the gradient of a potential function $P_{I_s}(x, y)$ computed from the image $I_s(x, y)$ of EM section s:

$$\mathbf{f}_i = \nabla P_{I_s}(\mathbf{x}_i) \tag{7}$$

where $\nabla = [\partial/\partial x, \partial/\partial y]'$. By simulating (1) with (7), the ravines (extended local minima) of P_{I_s} act as attractors to deformable contours. The contours descend and stabilize at the bottoms of the nearest ravines.

In the present application, we are interested in the localization of cell membranes, which appear dark in positive micrographs. We therefore convert $I_s(x, y)$ into a 2D potential function whose ravines coincide with dark cell membranes:

$$P_{I_s}(x, y) = G_\sigma * I_s(x, y) \tag{8}$$

where $G_\sigma *$ denotes convolution with a 2D Gaussian smoothing filter of width σ. The filter broadens the ravines of P_{I_s}, so that they attract the contours from some distance away.

In practice, I_s is not a continuous function, but a digital image. Therefore, we first convolve the image with a discrete smoothing kernel, then compute (7) by bilinearly interpolating the smoothed image gradients evaluated at the four pixels surrounding $\mathbf{x}_i$. The gradients are computed using forward finite differences of adjacent pixel values. The user can set the degree of smoothing σ and select the display of image I_s or potential functions P_{I_s} through a menu-driven interface.

The user initializes a closed deformable contour by quickly sketching with a mouse an approximate trace around the dark membrane of a dendrite of interest. Fig. 3(a) shows an initial deformable contour sketched near a cell membrane (nodes are created automatically so that they are spaced about one pixel apart, and an additional spring is inserted between the first and last nodes to close the contour). The user then initiates the snake simulation (5). In a few simulation time steps the deformable contour equilibrates at the bottom of the nearest ravine in P_{I_s} (Fig. 3(b)). By interacting with the contour (see below), the user can help it quickly localize the membrane ravine and conform to its shape to produce an accurate profile of the dendrite (Fig. 3(e)).

Because the dendritic profile is a closed continuous contour, it is easy to segment the interior of the cell from the rest of the image. We accomplish the segmentation by applying a standard region-fill algorithm [17] which starts from a seed point inside the profile and sequentially accesses the pixels of I_s that are bounded by the profile. Fig. 3(f) shows the dendritic profile segmented from the EM image in Fig. 3(e).

User and Constraint Forces: Often the user will sketch an initial trace which deviates too much from the membrane ravine to descend into the ravine properly. This is the case for the initial contour in Fig. 3(a) which reaches the equilibrium configuration shown in Fig. 3(b). As can be seen, the deformable contour may fall prey to nearby dark features inside the cell (or to nearby features of neighboring cells) which act as false attractors. In such a case, the user may apply interactive simulated forces $\mathbf{f}^{\mathbf{m}}{}_i(t)$ by using the mouse to guide the deformable contour towards the ravine of interest as it is stabilizing (see [32] for details about user forces). A useful force is the interactive spring

$$\mathbf{f}^{\mathbf{m}}{}_i = \begin{cases} \mathbf{x}_i - \mathbf{m}(t) & \text{if } \|\mathbf{x}_i - \mathbf{m}(t)\| \text{ is minimal for node } i, \\ 0 & \text{otherwise.} \end{cases} \tag{9}$$

which pulls the nearest node towards the time-varying mouse position $\mathbf{m}(t)$ in the image plane. Fig. 3(c) shows the effect of a user stretching the contour towards the right with an attached interactive spring (green line) from the mouse position (blue circle).

To localize a profile accurately, the user may want to constrain points on a deformable contour by attaching them with springs to selected anchor points on the image. Such constraints prevent the deformable contour from straying far from these points, regardless of the image forces and the user's other mouse manipulations. The mechanism for adding constraints is simply to fix $\mathbf{m}(t) = \mathbf{a}_k$ in the spring force (9) to create an anchor point $\mathbf{a}_k$ in the image. The constraining spring then applies a force $\mathbf{f}_i^{\mathbf{a}_k}$. Fig. 3(d) illustrates a constraint spring (blue line) which pulls the contour back towards an anchor point on the cell membrane as the user tugs on the contour with an interactive spring (green line). Note the two constraints (blue dots) in the final profile contour in Fig. 3(e).

Combining the three types of forces, we have

$$\mathbf{f}_i = c_I \nabla P_{I_s}(\mathbf{x}_i) + c_{\mathbf{m}} \mathbf{f}_i^{\mathbf{m}} + c_{\mathbf{a}} \sum_k \mathbf{f}_i^{\mathbf{a}_k} \tag{10}$$

where $\sum_k$ is a summation over all the anchor constraints in force and where c_I, $c_{\mathbf{m}}$, and $c_{\mathbf{a}}$ are the strength factors of the image forces, user spring forces, and anchor spring forces. We have determined empirically that the parameter values $c_{\mathbf{m}} = 0.02$, $c_{\mathbf{a}} = 0.02$, and $c_I = -0.002$ with P_{I_s} quantized in the range [0, 255] yield stable behavior and rapid convergence of deformable contours on cell membranes.

Exploiting Coherence Across Serial Sections: Our interactive technique for extracting cell profiles from EM images benefits from the fact that snakes can exploit the coherence of profile positions and shapes across adjacent images. Often, the user need not reinitialize the deformable contours when progressing from image to image to extract adjacent profiles of a dendrite.

Once the deformable contours equilibrate into the membrane ravines in P_{I_s}, we replace this potential function with the potential function $P_{I_{s\pm1}}$ of an adjacent member of the image sequence. Continuing from their previous equilibrium positions, the contours automatically descend into the new ravines to regain equilibrium, quickly localizing the new positions of the cell membranes in the adjacent image and conforming to their shapes.

This simple mechanism for exploiting image-to-image coherence works so long as the perturbation is small enough to maintain the deformable contours within the membrane ravines as we switch to adjacent images. Should part of a contour escape the ravine, however, the rest of the contour will usually pull it back into place due to the elasticity of the model.

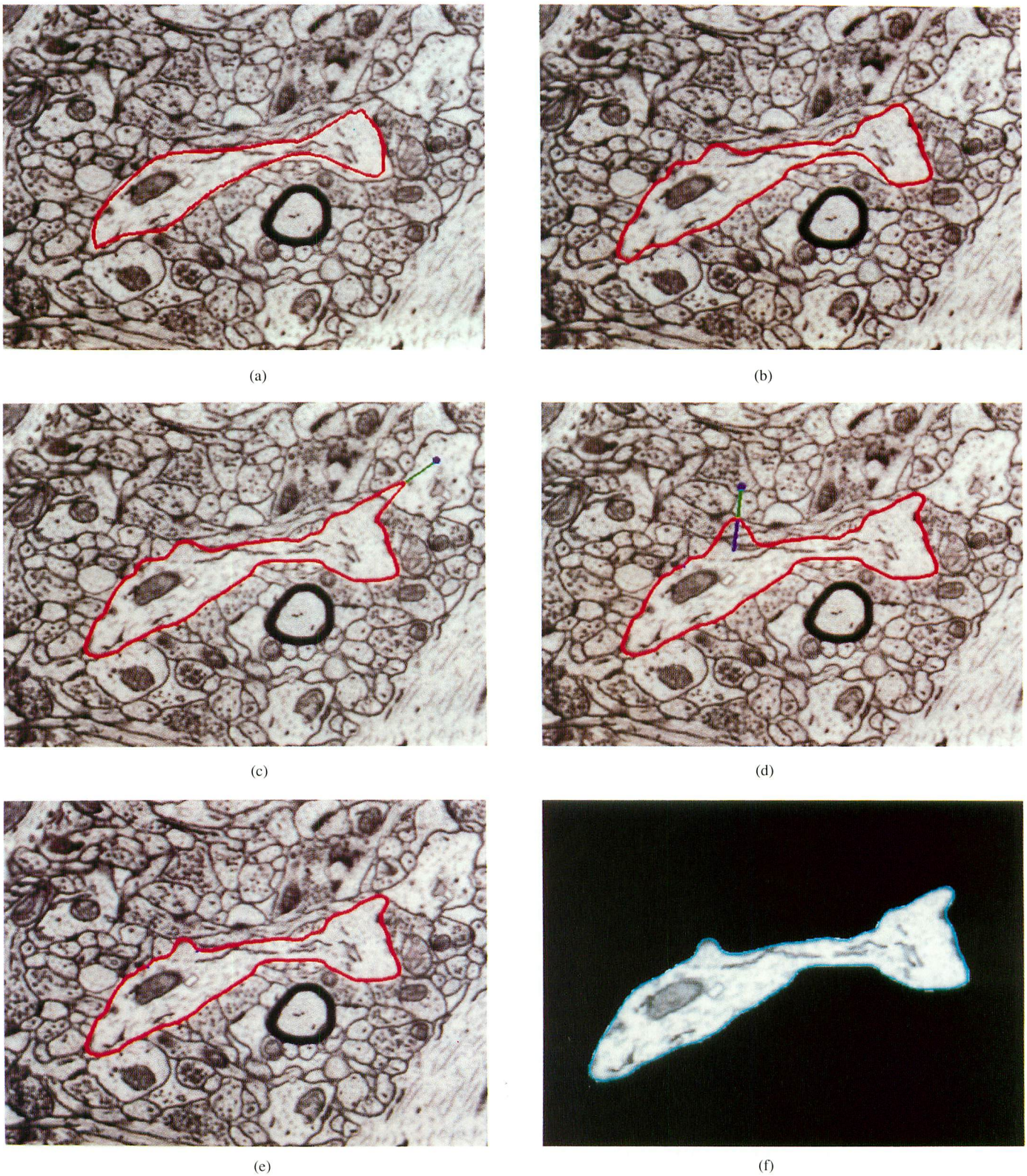

Fig. 3. Cell segmentation of the section in Fig. 2 using a deformable contour (see text). (a) Initial sketched contour. (b) Initial equilibrium position. (c)–(d) Manipulating the contour with interactive springs (green lines) and constraints (blue lines). (e) Final profile. (f) Segmented cell.

Contour Bifurcation and Mergence Operations: As we progress through consecutive sections, the dendritic spines may become disconnected from the parent dendrite, or disconnected spines may merge with the parent dendrite. To handle these situations efficiently, we have incorporated snake bifurcation and mergence operations that obviate snake reinitializations. The user may split a closed snake into two closed snakes and vice versa by simply using the mouse to

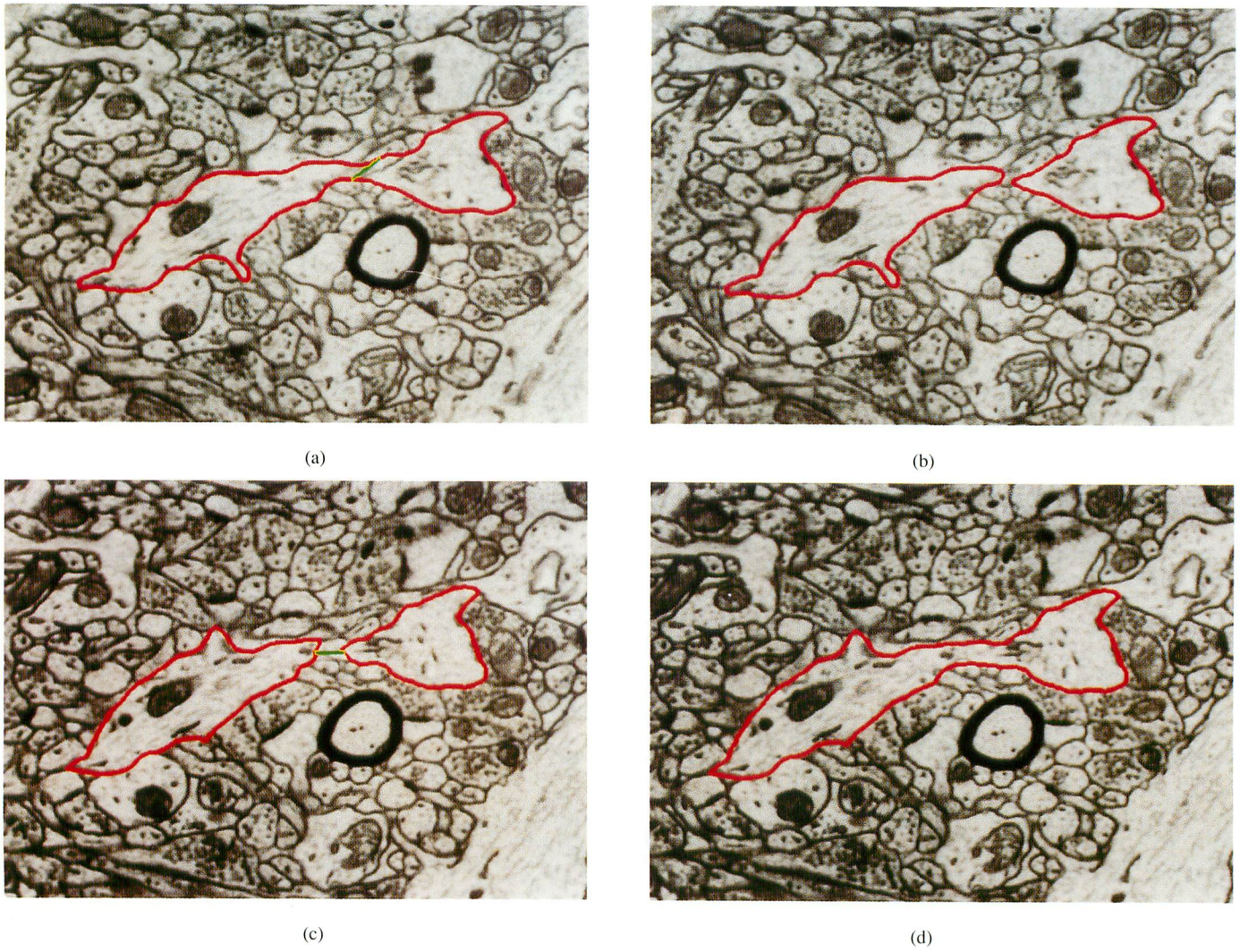

Fig. 4. Contour bifurcation and mergence (see text). (a) Snake to be bifurcated showing the two selected cut points connected by green line. (b) Bifurcated snakes conforming to the membranes of the dendrite and the separated spine. (c) Two snakes to be merged showing the selected cut points connected by green line. (d) Merged snake conforming to the membrane of the dendrite and connected spine.

select snake nodes. In the case where a spine separates from the parent dendrite, the user selects two cutting points on the snake (Fig. 4(a)) and the program automatically bifurcates the snake into two snakes which close and separately proceed to conform to their associated membranes (Fig. 4(b)). In the case where a spine joins the parent dendrite, the user selects a cutting point on each closed snake (Fig. 4(c)) and the program automatically opens and merges the snakes into one closed snake which proceeds to conform to the membrane boundary (Fig. 4(d)).

III. Visualizing Neuronal Dendrites

During image segmentation, the user can visualize what takes place in two graphics windows (Fig. 5). One window shows the current EM image overlayed with the graphics generated by the deformable contour simulation. The other window displays a stack of dendritic profiles and their interiors. The user can also see the current contour with the (partial) model, thereby monitoring progress. The stacked set of profiles and interiors can be rotated and viewed from different vantage points. A deformable contour in one window can be inserted as a profile into the other window and vice versa. When all the dendritic profiles have been extracted, we use the segmented dendritic interior to build a volumetric voxel model. We apply volume rendering techniques to visualize the volumetric model.

Volume rendering refers to the direct rendering of scalar data sampled in three dimensions. These techniques differ from traditional computer graphics techniques in that explicit surfaces need not be extracted from the data before display. Rather, the entire 3D volume of data is used for display. Yet, by displaying only the portions of the volume that have a given density or a high gradient, features and surfaces may be elicited without explicit representation [17].

We use the VoxelView^{TM} system [68] to reconstruct a 3D volumetric model of a dendrite from the dendritic interiors that have been segmented from the serial sections. The segmented dendrite in each image is enclosed by a rectangular array of black pixels. The resulting arrays, or images, are stacked in order. The sizes of the rectangular arrays are chosen so that the

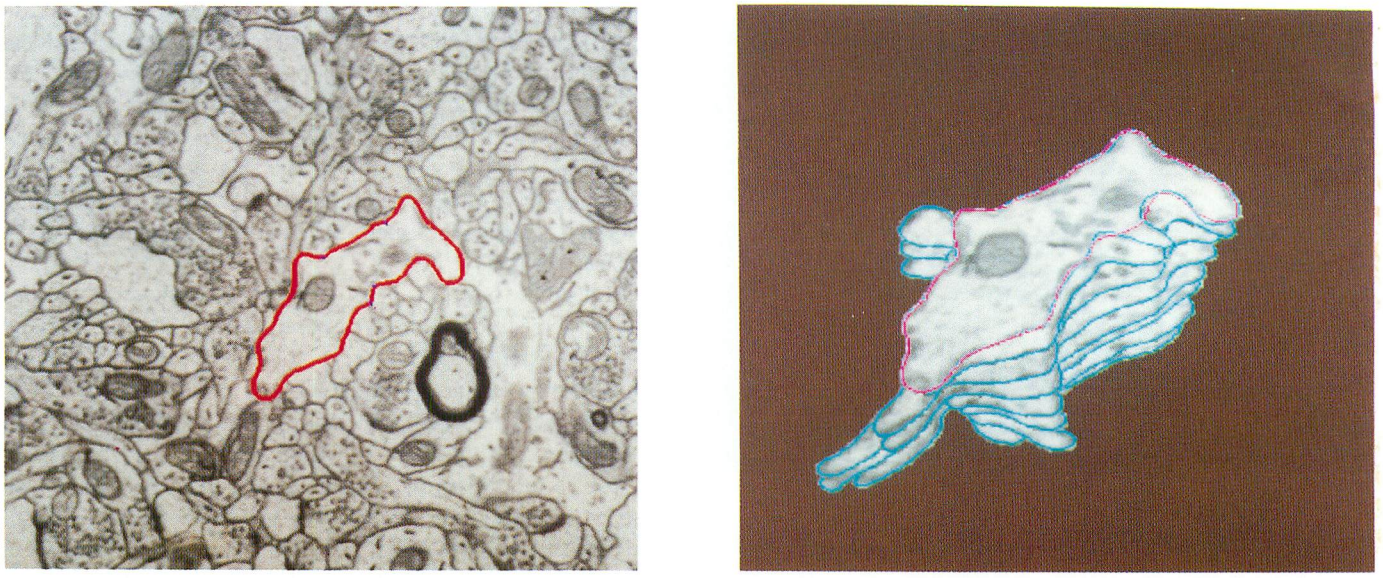

(a) (b)

Fig. 5. The two visualization windows. (a) The current EM image with an overlayed active deformable contour (snake). (b) A stack of dendritic profiles and their interiors. The active snake is displayed in red.

stack yields a rectangular parallelepiped. Since the sampling rate is less in the stacking direction (z-direction) than in the x- and y-directions of the images, the VoxelView^{TM} system linearly interpolates an additional number of sections. In the examples shown below, we have reconstructed 41 sections of a dendrite, and interpolated three sections between each pair of original sections to get approximately the correct proportions along the z-axis as we view all the sections.

By rapidly moving from one image to the next, we generate an interactive "movie" that enables us to follow certain features of interest through the dendrite. We can also slice the stack of images along planes perpendicular to the stacking direction, and along any arbitrary plane. Because of the tissue cutting direction, the dendrite is positioned obliquely in the image volume; therefore, we must cut the image volume obliquely to slice the dendrite lengthwise. One such oblique slice is shown in Fig. 6, where we can see the shape and extent of the mitochondrion through the dendrite, and also some smooth endoplasmic reticulum.

By default, the volume is rendered without any shading; however, the user can specify the position of a light source and obtain a shaded view of the model. In Fig. 7, we have rendered the dendrite model with shading. The shading helps accentuate the 3D shape of the dendrite.

For rapid volume rendering we also use a parallel ray-tracer implemented on a DECmpp^{TM} 12000/Sx massively parallel computer. The ray-tracing algorithm differs from previous methods [55] by holding the data stationary while accumulating the opacity along the rays in parallel. The 3D volumetric models can be interactively rotated and viewed translucently. Fig. 8 shows a translucent ray-traced image of the neuron model, which allows us to visualize how the mitochondrion extends through the dendrite. This model has been reconstructed using fractional section interpolation in order to obtain accurate proportions in the x-, y-, and z-directions.

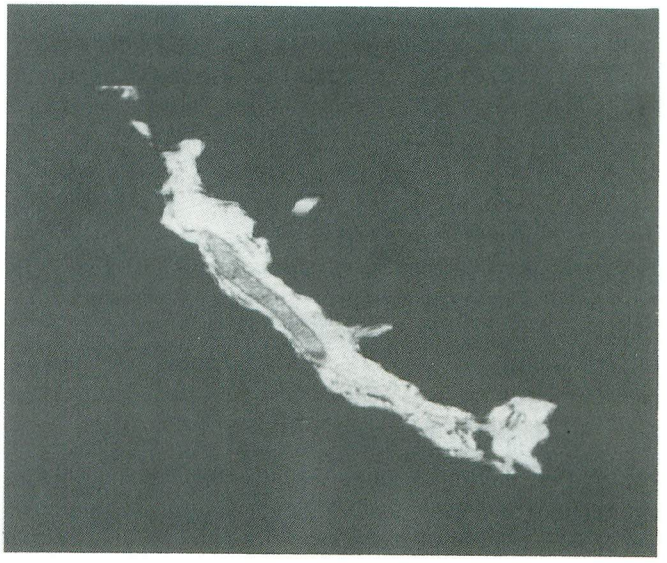

Fig. 6. Oblique slice through the model of a dendritere constructed from the 41 EM serial sections. The mitochondrion can be seen extending through the length of the dendrite and some smooth endoplasmic reticulum is visible in the large spine. Note that this section is oblique to the original EM sections. Therefore, this view is not present in the original data, but has been digitally reconstructed.

By using a volumetric representation of the dendritic model, we can represent the 3D shape of the model with accuracy limited only by the original sampling of the EM images. Furthermore, we can visualize the cytoskeleton and the organelles interior to the dendrite.

IV. Summary and Future Research

We have described components of a prototype system for the reconstruction and analysis of neuronal dendrites. Our goal is to reduce the effort required to reconstruct and analyze a

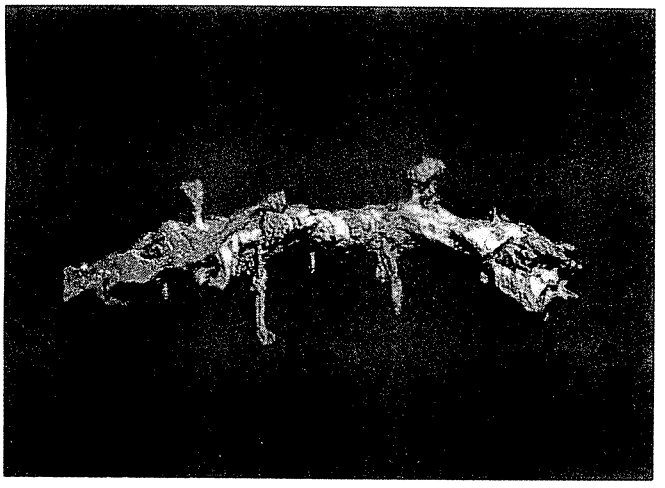

Fig. 7. Shaded model of the reconstructed dendrite.

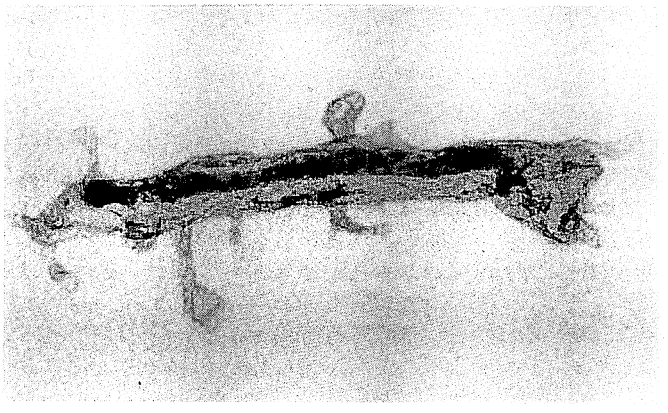

Fig. 8. Translucent model of the dendrite as reconstructed from the EM images. Unlike conventional images of internal substructures which are rendered as translucent surfaces in empty space, this image is rendered directly from a model which includes all of the EM voxel data contained within the dendritic membrane.

complete dendrite from months to days. We are approaching this goal by exploiting three recently developed techniques for volume reconstruction: a digital blink comparator for EM section registration, snakes, or active energy-minimizing contours, for dendrite segmentation, and volume rendering to visualize both the overall morphology of 3D dendrites and their cytoskeleton and internal organelles. The image registration and segmentation tools in our system run at interactive rates on modern graphics workstations with no special purpose hardware.

Some work remains to be done to improve the reconstruction process. The digital blink comparator opens a way to use direct digitization from electron microscopes for serial microscopy. This would eliminate the need for rephotographing and digitizing EM photomicrographs, thus reducing the reconstruction time and eliminating distortions and quantization errors introduced by these processes. Direct digitization from an electron microscope has been used for single section studies, but has until now been impossible to use for serial microscopy, which requires section alignment [60].

We need to provide (at least) a semiautomatic approach to image registration, with the user intervening only for optional fine-tuning. Currently, during manual alignment, we resample the image using nearest pixel sampling. It would be desirable, however, to allow subpixel alignment and resampling by using a spatially varying shift filter, but this is computationally prohibitive with our current equipment. Despite the sampling limitations, we have found the resulting alignments to be quite satisfactory.

We need to improve upon interpolation between sections during reconstruction and between voxels during volume slicing and rendering in order to reduce aliasing without compromising image accuracy.

We have not yet begun to address the anatomical analysis of dendrites. To this end, it would be useful to reconstruct 3D surface models from a set of stacked planar profiles (such as the set illustrated in Fig. 5) that have been extracted from the serial electron micrographs using snakes. The snakes yield profiles as lists of vertices in space, a representation that may be input to any of a number of existing algorithms for reconstructing surfaces from planar cross sections ([34], [19], [11], [20], [3], [41], [21], [57]). The deformable cylinder model developed in [63] may also be adapted to this surface reconstruction task. We expect that through semiautomated approaches for dendrite decomposition, anatomical measurements, and statistical analysis of these measurements, we can achieve reductions in analysis times similar to those that we are beginning to realize in the reconstruction phase.

When we add rapid image acquisition and quantitative analysis components to our system, it will be possible to obtain a sufficiently large number of reconstructions to evaluate quantitatively the functional consequences that alterations in neuronal morphology have for both the normal and diseased brain.

ACKNOWLEDGMENT

The authors would like to thank Victor Vyssotsky, Director of Digital Equipment Corporation's Cambridge Research Lab, for his support of this research. William Hsu implemented the volume ray-tracer on the DECmpp^{TM} 12000/Sx. This work has benefited from many discussions with Gudrun Klinker and Richard Szeliski, and from the use of image conversion software written by Richard Szeliski. We would like to thank Robert Ulichney and Victor Bahl for their help with the Autokon scanner. We also thank Dick Beane, Gudrun Klinker, and Richard Szeliski for reading and commenting on the manuscript.

REFERENCES

[1] R. S. Aikens, D. A. Agard, and J. W. Sedat, "Solid-state imagers for microscopy," *Methods in Cell Biology*, Y. L. Wang and D. L. Taylor, Eds., New York: Academic Press, Inc., 1989, vol. 29, pp. 291–313.

[2] N. Ayache, J. D. Boissonnat, E. Brunet, L. Cohen, J. P. Chieze, B. Geiger, O. Monga, J. M. Rocchisani, and P. Sander, "Building highly structured volume representations in 3D medical images," in *Proc. 3rd Int. Symp. on Computer Assisted Radiology, CAR'89*, New York: Springer-Verlag, 1989, pp. 765–772,.

[3] J. D. Boissonnat, "Shape reconstruction from planar cross-sections." *Comput. Vision, Graphics and Image Processing*, vol. 44, pp. 1–29, Oct. 1988.

[4] C. Bron, P. Gremille, D. Launey, M. Jourlin, H. P. Gautschi, T. Bächi, and J. Schüpbach. "Three-dimensional electron microscopy of entire cells," *J. Microscopy*, vol. 157, pp. 115–126, Jan. 1990.

[5] T. H. Brown, V. C. Chang, A. H. Ganong, C. L. Keenan, and S. R. Kelso, "Biophysical properties of dendrites and spines that may control the induction and expression of long-term synaptic potentiation," *Neurology and Neurobiology*, vol. 35, pp. 201–264, 1988.

[6] T. H. Brown, P. F. Chapman, E. W. Kairiss, and C. L. Keenan, "Long-term synaptic potentiation," *Sci.*, vol. 242, pp. 724–728, Nov. 1988.

[7] J. P. Byrne, P. E. Undrill, and R. P. Phillips. "Feature based image registration using parallel computation methods," in *First Conf. on Visualization in Biomedical Computing*, Los Alamitos, CA: IEEE Computer Society Press, 1990, pp. 304–310.

[8] I. Carlbom, D. Terzopoulos, and K. M. Harris. "Reconstructing and visualizing models of neuronal dendrites," *Scientific Visualization of Physical Phenomena*, N. M. Patrikalakis, Ed., pp. 623–638. New York: Springer-Verlag, Tokyo, 1991. Also presented at *CG International '91: Visualization of Physical Phenomena*, 991.

[9] I. Catala, I. Ferrer, E. Galofre, and I. Fabreques. "Deceased numbers of dendritic spines on cortical pyramidal neurons in dementia: A quantitative Golgi study on biopsy samples," *Human Neurobiology*, vol. 6, pp. 255–259, 1988.

[10] I. Chakravarty, B. Nichol, and T. Ono, "The integration of computer graphics and image processing techniques for the display and manipulation of geophysical data," in *Proc. Comput. Graphics Tokyo '86*, 1986. Reprinted in *Advanced Computer Graphics*, T. Kunii, Ed., New York: Springer-Verlag, 1986.

[11] H. N. Christiansen and T. W. Sederberg, "Conversion of complex contour line definitions into polygonal element mosaics," *Comput. Graphics*, vol. 12, pp. 187–192, 1982.

[12] K. Croswell. "The pursuit of Pluto." *Am. Heritage of Invention and Technol.*, vol. 5, no. 3, pp. 50–57, 1990.

[13] R. A. Drebin, L. Carpenter, and P. Hanrahan. "Volume rendering." *Comput. Graphics*, vol. 22, no. 4, 65–74, Aug. 1988.

[14] J. S. Duncan, L. H. Staib, T. Birkholzer, R. Owen, P. Anandan, and I. Bozma, "Medical image analysis using model-based optimization," in *First Conf. on Visualization in Biomedical Computing*, Los Alamitos, CA: IEEE Computer Society Press, 1990, pp. 370–377.

[15] M. L. Feldman and C. Dowd, "Loss of dendritic spines in aging cerebral cortex," *Anatomy and Embryology*, vol. 148, pp. 279–301, 1975.

[16] I. Ferrer, I. Fabreques, J. Rairiz, and E. Galofre, "Decreased numbers of dendritic spines on cortical pyramidal neurons in human chronic alcoholism," *Neurosci. Lett.*, vol. 69, pp. 115–119, 1986.

[17] J. D. Foley, A. van Dam, S. K. Feiner, and J. F. Hughes, *Computer Graphics: Principles and Practice*. Reading, MA: Addison-Wesley Publishing Company, 1990.

[18] R. E. Frederiksen, J. M. Coggins, T. J. Cullip, and S. M. Pizer, "Interactive object definition in medical images using multiscale, geometric image descriptions," in *First Conf. on Visualization in Biomedical Computing*, Los Alamitos, CA: IEEE Computer Society Press, pp. 108–114, 1990.

[19] H. Fuchs, Z. M. Kedem, and S. P. Uselton, "Optimal surface reconstruction from planar contours," *Commun. ACM*, vol. 20, no. 10, pp. 693–702, 1977.

[20] S. Ganapathy and T. G. Dennehy, "A new general triangulation method for planar contours," *Comput. Graphics*, vol. 16, pp. 69–75, 1982.

[21] C. Giertsen, A. Halvorsen, and P. R. Flood, "Graph-directed modeling from serial sections," *The Visual Comput.*, vol. 6, no. 5, pp. 284–290, Nov. 1990.

[22] G. Graveland, R. S. Williams, and M. DiFiglia, "Evidence for degenerative and regenerative changes in neostriatal spiny neurons in Huntington's disease," *Sci.*, vol. 227, pp. 770–773, 1985.

[23] K. M. Harris, W. L. R. Cruce, W. T. Greenough, and T. J. Teyler, "A Golgi impregnation technique for thin brain slices maintained in vitro," *J. Neurosci. Methods*, vol. 2, pp. 363–371, 1980.

[24] K. M. Harris, F. E. Jensen, and B. H. Tsao, "Ultrastructure, development, and plasticity of dendritic spine synapses in area CA1 of the rat hippocampus: Extending our vision with serial electron microscopy and three-dimensional analysis," *Neurology and Neurobiology*, vol. 52, pp. 33–52, 1989.

[25] K. M. Harris and J. K. Stevens, "Dendritic spines of rat cerebellar Purkinje cells: Serial electron microscopy with reference to their biophysical characteristics," *J. Neurosci.*, vol. 8, no. 12, pp. 4455–4469, Dec. 1988.

[26] K. M. Harris and J. K. Stevens, "Dendritic spines of CA1 pyramidal cells in the rat hippocampus: Serial electron microscopy with reference to their biophysical characteristics," *J. Neurosci.*, vol. 9, no. 8, pp. 2982–2997, Aug. 1989.

[27] D. Hessler, S. J. Young, B. O. Carragher, M. E. Martone, S. Lamont, M. Whittaker, R. A. Milligan, E. Masliah, J. E. Hinshaw, and M. H. Ellisman, "Programs for visualization in three-dimensional microscopy," *Neuroimage*, vol. 1, no. 1, pp. 55–67, 1992.

[28] B. K. P. Horn, *Robot Vision*. Cambridge, MA: The MIT Press, 1986.

[29] K. H. Höhne, M. Bomans, A. Pommert, M. Riemer, C. Schiers, U. Tiede, and G. Wiebecke, "3D visualization of tomographic volume data using the generalized voxel-model," *Proc. Volume Visualization Workshop*, C. Upson, Ed., pp. 51–57, Department of Computer Science, University of North Carolina, Chapel Hill, NC, 1989.

[30] K. H. Höhne, M. Bomans, A. Pommert, M. Riemer, and U. Tiede, "3D segmentation and display of tomographic imagery," in *Proc. Int. Conf. Pattern Recognition*, Los Alamitos, CA: IEEE Computer Society Press, 1988, pp. 1271–1276.

[31] E. R. Kandel and J. H. Schwartz, *Principles of Neural Science*. New York: Elsevier Science Publishing Co., Inc., 1985.

[32] M. Kass, A. Witkin, and D. Terzopoulos, "Snakes: Active contour models," *Int. J. Comput. Vision*, vol. 1, no. 4, pp. 321–331, 1987.

[33] A. Kaufman, R. Yagel, R. Bakalash, and I. Spector, "Volume visualization in cell biology." in *Proc. Visualization'90*, A. Kaufman, Ed., Los Alamitos, CA: IEEE Computer Society Press, pp. 160–167, 1990.

[34] E. Keppel "Approximating complex surfaces by triangulation of contour lines," *IBM Res. and Develop.*, vol. 19, pp. 2–11, 1975.

[35] C. Koch, A. Zador, and T. H. Brown "Dendritic spines: Convergence of theory and experiment," *Sci.*, vol. 256, pp. 973–974, May 1992.

[36] R. J. Lasek and M. M. Black, *Intrinsic Determinants of Neuronal Form and Function*. New York: Alan R. Liss, Inc., 1988.

[37] F. Leitner, I. Marque, S. LaVallee, and P. Cinquin, "Dynamic segmentation: Finding the edge with differential equations and 'spline snakes'," *Technical Report TIMB-TIM 3-IMAG*, Faculte de Medecine, 38700 La Tronche, France, 1990.

[38] M. Levoy, "Efficient ray-tracing of volume data," *ACM Trans. Graphics*, vol. 9, no. 3, pp. 245–261, July 1990.

[39] F. Leymarie, "Tracking and describing deformable objects using active contour models," *Master's thesis*, Computer Vision and Robotics Laboratory, McGill Research Centre for Intelligent Machines, McGill University, Montreal, Canada, Feb. 1990.

[40] L. M. Lifshitz and S. M. Pizer. "A multiresolution hierarchical approach to image segmentation based on intensity extrema," *IEEE Trans. Pattern Anal. and Mach. Intell.*, vol. 12, no. 6, pp. 529–540, June 1990.

[41] W. C. Lin, S. Y. Chen, and C. T. Chen, "A new surface interpolation technique for reconstructing 3D objects from serial cross sections," *Comput. Vision Graphics and Image Processing*, vol. 48, pp. 124–143, 1989.

[42] P. Lipson, A. L. Yuille, D. O. O'Keeffe, J. Cavanaugh, J. Taaffe, and D. Rosenthal, "Automated bone density calculation using feature extraction by deformable templates," In *First Conf. Visualization in Biomedical Computing*, 1990, pp. 477–484, 1990. IEEE Computer Society Press, Los Alamitos, CA.

[43] H. K. Liu, "Two and three dimensional boundary detection," *Comput. Graphics and Image Processing*, vol. 6, pp. 123–134, 1977.

[44] W. E. Lorensen and H. E. Cline, "Marching cubes: A high resolution 3D surface construction algorithm," *Comput. Graphics*, vol. 21, no. 4, pp. 163–169, July 1987.

[45] M. Marin-Padilla, "Pyramidal cell abnormalities in the motor cortex of a child with Down's syndrome," A Golgi study, *J. Comput. Neurology*, vol. 167, pp. 63–82, 1976.

[46] D. Meagher, "Geometric modeling using octree encoding," *Comput. Graphics and Image Processing*, vol. 19, pp. 129–147, 1982.

[47] D. Meagher, "Interactive solids processing for medical analysis and planning," in *Proc. Nat. Comput. Graphics Association, NCGA'84*, 1984.

[48] D. G. Morgenthaler and A. Rosenfeld, "Multidimensional edge detection by hypersurface fitting," *IEEE Transactions on Pattern Analysis and Machine Intelligence*, vol. 3, no. 4, pp. 482–486, July 1981.

[49] A. V. Oppenheim and R. W. Schafer, Digital Signal Processing. Englewood Cliffs, NJ: Prentice Hall, Inc., 1975.

[50] W. H. Press, B. P. Flannery, S. A. Teukolsky, and W. T. Vetterling. Numerical Recipes: The Art of Scientific Computing. Cambridge, U.K: Cambridge University Press, 1986.

[51] W. Rall, "Dendritic spines, synaptic potency and neuronal plasticity," *Cellular Mechanisms Subserving Changes in Neuronal Activity*, in C. Woody, K. Brown, T. Crow, and J. Knispel, Eds., Los Angeles, CA, Brain Information Service, 1974, pp. 13–21. .

[52] P. Sabella, "A rendering algorithm for visualizing 3D scalar fields," *Comp. Graphics*, vol. 22, no. 4, pp. 51–58, Aug. 1988.

[53] P. T. Sander and S. W. Zucker, "Inferring surface trace and differential structure from 3-D images," *IEEE Trans. Pattern Anal. and Mach. Intell.*, vol. 12, vol. 9, pp. 833–854, Sept. 1990.

[54] M. E. Scheibel, P. H. Crandall, and A. B. Scheibel, "The hippocampal-dentate complex in temporal lobe epilepsy," *Epilepsia*, vol. 15, pp. 55–80, 1940.
[55] P. Schröder and J. B. Salem, "Fast rotation of volume data on data parallel architectures," *Proc. Visualization'91*, in G. M. Nielson and L. Rosenblum, Eds., Los Alamitos, CA: IEEE Computer Society Press, 1991, pp. 50–57.
[56] S. L. Senft, V. J. Argiro, and W. L. VanZandt, "Volume microscopy of biological speciments based on non-confocal imaging techniques," in *Proc. Visualization'90*, A. Kaufman, editor, Los Alamitos, CA: IEEE Computer Society Press, 1990.
[57] Y. Shinagawa and T. L. Kunii, "The homotopy model: A generalized model for smooth surface generation from cross sectional data," *The Visual Comput.*, vol. 7, no. 2, pp. 72–86, May 1991.
[58] J. Spacek, "Ultrastructural pathology of dendritic spines in epitumorous human cerebral cortex," *Acta Neuropathology*, vol. 73, pp. 77–85, 1987.
[59] J. K. Stevens, T. L. Davis, N. Friedman, and P. Sterling, "A systematic approach to reconstructing microcircuitry by electron microscopy of serial sections," *Brain Res. Rev.*, vol. 2, pp. 265–293, 1980.
[60] J. K. Stevens and J. Trogadis, "Computer-assisted reconstruction from serial electron micrographs: A tool for the systematic study of neuronal form and function," *Advances in Cellular Neurobiology*, vol. 5, pp. 341–369, 1984.
[61] J. K. Stevens and J. Trogadis, "A systematic approach to 3D confocal microscopy: Application of volume investigation methods," *J. Microscopy*, in press, 1994.
[62] D. Terzopoulos, "On matching deformable models to images: Direct and iterative solutions," in *Topical Meeting on Machine Vision*, Optical Society of America, 1987, pp. 160–16.
[63] D. Terzopoulos, A. Witkin, and M. Kass, "Constraints on deformable models: Recovering 3D shape and nonrigid motion," *Artificial Intell.*, vol. 36, no. 1, pp. 91–123, Aug. 1988.
[64] R. Ulichney. *Image Lab Picture Files, Internal Memo.* Digital Equipment Corporation, Maynard, MA, 1982.
[65] C. Upson, Ed., Proc. Chapel Hill Workshop on Volume Visualization. Department of Computer Science, University of North Carolina, Chapel Hill, NC, May 1989.
[66] C. Upson, T. Faulhaber Jr., D. Kamins, D. Laidlaw, D. Schlegel, J. Vroom, R. Gurwitz, and A. van Dam, "The application visualization system: A computational environment for scientific visualization," *IEEE Comput. Graphics and Applicat.*, vol. 9, no. 4, pp. 30–42, July 1989.
[67] K. L. Vincken, C. N. de Graaf, A. S. E. Koster, M. A. Viergever, F. J. R. Appelman, and G. R. Timmens, "Multiresolution segmentation of 3D images by the hyperstack," in *First Conf. Visualization in Biomedical Computing*, Los Alamitos, CA: IEEE Computer Society Press, pp. 115–122, 1990.
[68] *VoxelView/PLUS 1.4, The interactive volume rendering system.* VitalImages, Inc., Fairfield, IA, 1990.
[69] J. Wickens, "Electrically coupled but chemically isolated synapses: Dendritic spines and calcium in a rule for synaptic modification," *Progress in Neurobiology*, vol. 31, pp. 507–528, 1988.
[70] C. J. Wilson, F. Murakami, H. Katsumaru, and N. Tsukahara, "Dendritic and somatic appendages of identified rubrospinal neurons of the cat," *Neurosci.*, vol. 22, pp. 113–130, 1987.
[71] G. Wolberg. *Digital Image Warping.* Los Alamitos, CA: IEEE Computer Society Press, 1990.
[72] R. H. Wolphe Jr. and C. N. Liu, "Interactive visualization of 3D seismic data: A volumetric method," *IEEE Comput. Graphics and Applicat.*, vol. 8, pp. 24–30, July 1988.
[73] S. W. Zucker and R. A. Hummel, "A three-dimensional edge operator," *IEEE Trans. Pattern Anal. and Mach. Intell.*, vol. 3, pp. 324–331, May 1981.